Dynamic response of the Chamousset rock column (Western Alps, France)

Clara Lévy, L. Baillet, D. Jongmans, P. Mourot, D. Hantz

Dynamic response of the Chamousset rock column (Western Alps, France)

C. Lévy,[1] L. Baillet,[1] D. Jongmans,[1] P. Mourot,[2] and D. Hantz[1]

Received 20 November 2009; revised 17 September 2010; accepted 27 September 2010; published 31 December 2010.

[1] This paper investigates the variation of the first resonance frequency of the Chamousset limestone column (21,000 m^3, Vercors, French Alps) before its collapse in November 2007. The site was instrumented with seismometers and extensometers during a 4-month period with some gaps in the measurements. Experimental results and numerical modeling showed that the resonance frequency of a prone-to-fall column can be derived from the spectra of continuous seismic noise records. At the Chamousset site, the evolution of the resonance frequency appeared to be strongly controlled by the temperature. When temperatures were positive, slight resonance frequency variations correlated well with thermal fluctuations. Irreversible damage can occur during freeze-thaw cycles and to a lesser extent during strong wind. It coincided with a significant drop in resonance frequency, which was interpreted as the result of rock bridge breakage. This hypothesis is supported by fresh rupture observations after the collapse, seismic event records, and numerical modeling. This study suggests that seismic noise recording could be used for assessing the potential failure of unstable columns in rigid rocks.

Citation: Lévy, C., L. Baillet, D. Jongmans, P. Mourot, and D. Hantz (2010), Dynamic response of the Chamousset rock column (Western Alps, France), *J. Geophys. Res.*, *115*, F04043, doi:10.1029/2009JF001606.

1. Introduction

[2] Rock failure assessment requires the detection of the unstable volume and the prediction of the rupture phase [*Crosta and Agliardi*, 2003]. The failure mechanism is strongly controlled by the geological and structural conditions of the mass and the slope morphology [*Hoek and Bray*, 1981]. Performing traditional fieldwork on a rock face can pose huge problems of accessibility, safety, and data quality. Consequently, terrestrial and airborne remote sensing techniques have been increasingly used for generating a digital elevation model (DEM) of rock slopes and to extract quantitative and valuable information on the discontinuity pattern affecting the rock face [among others, *Jaboyedoff et al.*, 2004; *Deparis et al.*, 2008a; *Sturzenegger and Stead*, 2009]. Besides the fact that it is not restricted to single measurement points, laser scanning allows the structural analysis of steep and inaccessible slopes to be made. The unstable volume geometry and potential failure mechanism can be roughly estimated by extrapolating the joints extracted from DEM [*Oppikofer et al.*, 2009; *Sturzenegger and Stead*, 2009].

[3] However, such measurements do not provide information about the internal structure of the rock mass. Back analysis of 25 rock falls in steep limestone cliffs in the French Alps [*Frayssines and Hantz*, 2006] showed that these events were initiated by intact rock failure in rock bridges and that the persistence of joints was the main factor to consider in the evaluation of failure probability. A few percentage points of remaining rock bridges out of the whole contact surface are usually sufficient for stability. Rock bridge mapping is then a crucial step for rock failure assessment. In the past few years, several authors [*Jeannin et al.*, 2006; *Roch et al.*, 2006; *Deparis et al.*, 2008a] have applied geophysical techniques for delineating and characterizing the joint pattern inside the rock mass. It turned out that ground penetrating radar (GPR) profiles conducted on the cliff face yielded the best results in terms of penetration and resolution and provided the geometry and continuity of the major open joints. However, besides the difficulty of deployment on a cliff, the GPR method offers the disadvantages to be limited to high resistive rock slopes (owing to the poor radar wave penetration in electrically conductive material) and to sites where abseiling is feasible. Hence, the technique can only be applied for specific surveys.

[4] Contrary to other landslide types, rock falls are usually sudden phenomena with few apparent precursory patterns observed prior to the collapse. The forecast of rock slope failure and the search of precursors have been an active research topic for the past decade with applications in rock mechanics, rock engineering, and mining [*Zvelebil and Moser*, 2001; *Crosta and Agliardi*, 2003; *Amitrano et al.*, 2005; *Wu et al.*, 2006; *Rosser et al.*, 2007; *Oppikofer et al.*, 2008; *Lato et al.*, 2009]. The most common observed precursors have been accelerations of the fracture opening [*Voight and Kennedy*, 1979; *Azimi and Desvarreux*, 1996;

[1]Laboratoire de Géophysique Interne et Tectonophysique, CNRS, Grenoble University, France.
[2]Myotis Society, Saint Martin d'Hères, France.

0148-0227/10/2009JF001606

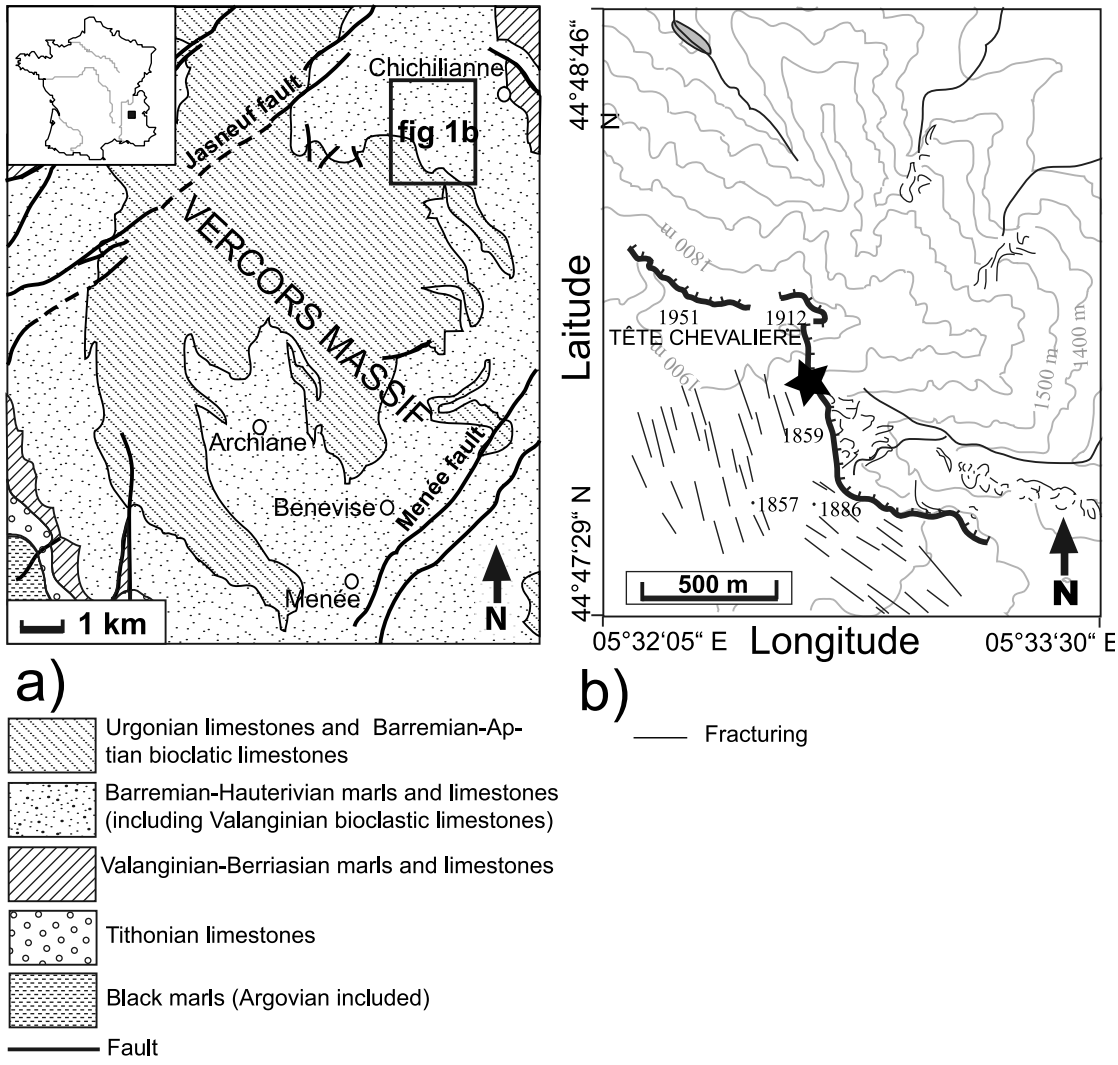

Figure 1. Location of the study site (Chamousset). (a) Geological map of the southern Vercors massif (France) (modified from *Gidon* [1977]). (b) Detailed topographic map (located by a rectangle in Figure 1a) showing the Chamousset site (star) at the top of the cliff.

Zvelebil and Moser, 2001] or of the ground displacement [*Crosta and Agliardi*, 2003; *Sornette et al.*, 2004; *Petley*, 2004; *Oppikofer et al.*, 2008]. These data were usually interpreted using the slope creep theory [*Saito and Uezawa*, 1961; *Fukuzono*, 1985; *Voight*, 1989; *Kilburn and Petley*, 2003], which allows for predicting the time of slope failure occurrence. At the present time, sequential laser scanning measurements easily enable the detection of failure-prone zones, which exhibit high displacement rates [*Oppikofer et al.*, 2008; *Lato et al.*, 2009]. Recently, *Rosser et al.* [2007] analyzed high-resolution sequential laser scanning data to identify spatial and temporal patterns in rock fall activity. Their results suggested that rock falls could potentially be viewed and quantified as precursors for larger slope failure.

[5] Seismic monitoring systems operating autonomously have been increasingly used for analyzing the seismicity induced by the mass movements and for locating the generated microearthquakes [*Amitrano et al.*, 2005; *Spillmann et al.*, 2007; *Mertl and Brückl*, 2007; *Amitrano et al.*, 2007; *Walter and Joswig*, 2008, 2009; *Amitrano et al.*, 2010; *Got et al.*, 2010; *Gaffet et al.*, 2010]. However, event identification, classification, and location turned out to be a complex task in rock gravitational movements, owing to the large number and the complex shape of recorded seismic events, as well as to the highly heterogeneous seismic structure [*Spillmann et al.*, 2007; *Mertl and Brückl*, 2007, *Walter and Joswig*, 2009]. Recently, *Burjánek et al.* [2010] deployed a small aperture seismic array for analyzing ambient vibrations on the unstable rock slope of Randa (Switzerland). Using a reference site on the stable part, they computed site-to-reference spectral ratios. They found amplification at sites located within the unstable part of the slope associated with polarization orientations in agreement with displacement directions.

[6] In the case of rock falls, *Amitrano et al.* [2005] seismically monitored a natural chalk cliff (Haute Normandie, France) before a 1–2 10^3 m^3 collapse. Looking for simple precursors, they observed a tremendous rising of seismic activity and energy a few hours prior to the fall, but only on

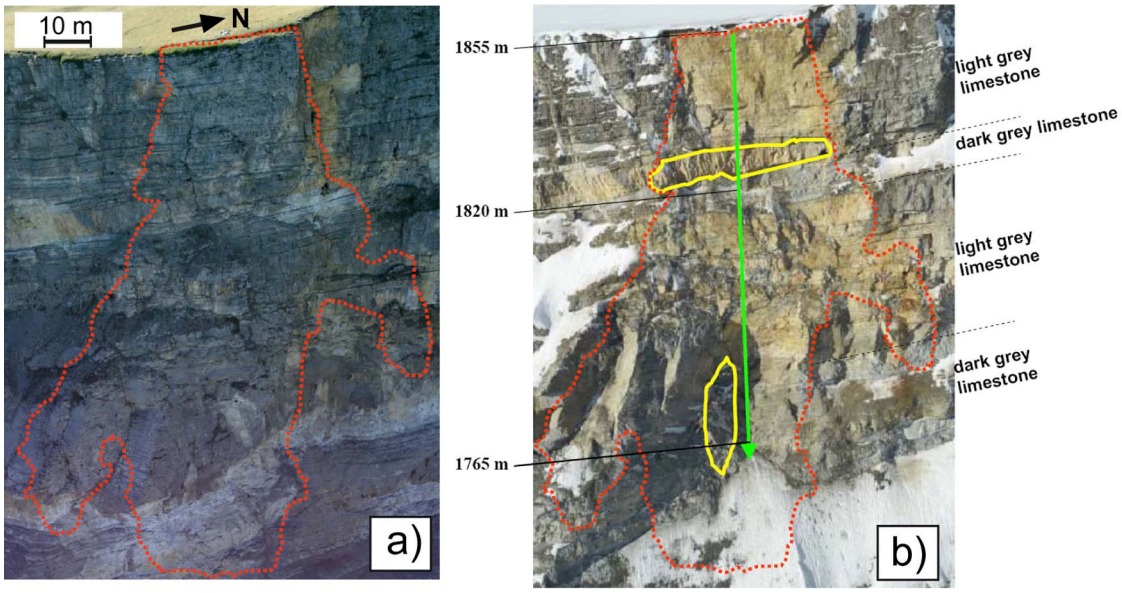

Figure 2. Photographs of the Chamousset cliff (a) prior to and (b) after the collapse. Limits of (a) the column and of (b) the rupture plane are shown in red dashed lines. (b) Rock bridges zones are shown in yellow. The abseiling path is shown with a green arrow in Figure 2b.

one close station located within one rupture length distance from the rock fall rupture plane. Working with the same data set, *Senfaute et al.* [2009] detected strong signals approximately 15 hours prior to a rock fall. They observed a progressive decrease of frequency spectrum for the microseismic events as the rock mass approached failure. These results enlighten observations made by other authors [*Azimi and Desvarreux*, 1996; *Rosser et al.*, 2007] during rock falls that most of the above-mentioned instability precursors remain stable until a few days, and more often a few hours, prior to a rock collapse, making long-term failure hazard assessment difficult. *Got et al.* [2010] monitored the displacement and seismic activity of an unstable rock column in a natural limestone cliff (Vercors massif, French Alps) during 3 months preceding its failure. However, the monitoring system stopped working 2 weeks before the collapse. Studying the seismic noise, they found a steady increase in the high-frequency base noise level and the emergence of spectral modes during the last weeks of operation.

[7] In this paper, we investigate the application of the seismic noise recorded by monitoring systems for evaluating the degree of coupling of a prone-to-fall column to the rock massif. During the past two decades, the use of seismic noise for modal analysis of structures has increased in civil engineering [for a recent review, see *Michel et al.*, 2008]. *Clinton et al.* [2006] processed continuous ambient vibration records to study the drop in the natural frequency of buildings, resulting from a decrease in system stiffness with the progressive damaging during earthquakes. Similarly, when a rock column decouples from the mass, the contact stiffness decreases with the breakage of rock bridges, resulting in natural frequency drop. We propose to use ambient noise array measurements to study the evolution of the natural frequencies of a rock column until its fall. Toward that purpose, we applied it to the limestone cliff of Chamousset (Vercors massif, France), which was also studied by *Got et al.* [2010]. Compared with this former work, our study is focused on the column natural frequency evolution and covers a longer time period, ranging from 6 months to 2 weeks prior to the collapse of 21,000 m^3. A significant natural frequency decrease was observed and was successfully numerically modeled using the geometry and the rock bridge location derived from the helicopter photos and scan laser images taken before and after the collapse.

2. Field Site: The Chamousset Rock Fall

[8] The Chamousset site is located at the top of the 300-m-high Urgonian cliff delineating the southern Vercors massif, French Alps (Figure 1a), which is affected by northeast trending strike-slip faults. In its upper part (highest 100 m), the facing east cliff is made of near-horizontally meter-thick bedded limestone (Figure 2b), while marly limestone composes the less steep lower part of the cliff where layers are a few decimeters thick. A structural study performed on the nearby outcrops on the plateau showed that layers at the meter scale are affected by two near-vertical fracture sets striking N110–120°E and N30–50°E. The latter set is parallel to the strike-slip faulting. At the hectometer scale, the mass is cut by N160° oriented near-vertical fracture planes (Figure 1b) which control the cliff orientation at the Chamousset site.

[9] A limestone column of 21,000 m^3 felt down from the upper part of the cliff the 24 November 2007 (personal communication of an inhabitant of the village of Chichilianne, Figure 1a). Figure 2 shows pictures taken before and after the fall. The collapse took place in late fall, when the Vercors plateau (1850 m to 1950 m of elevation in this area; Figure 1b) was covered by a 5-cm-thick layer of snow. Rangers of the regional park of the Vercors massif, who observed the progressive opening of a 30-m-long tension crack on the plateau, detected the unstable column. The crack opening was about 1 m before the collapse. Two

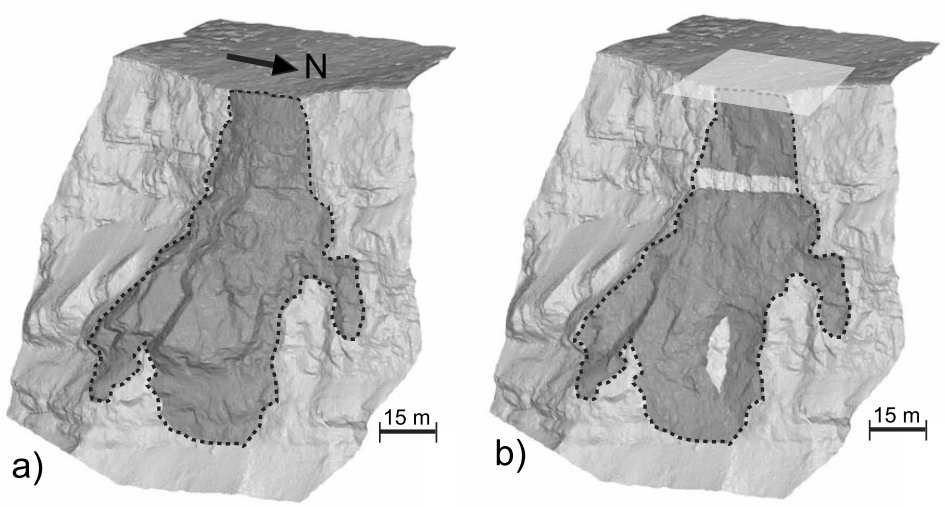

Figure 3. Digital elevation models of the cliff obtained from the lidar acquisitions. (a) Prior to the collapse. Rock column upper face is shown in dark shaded area. (b) After the collapse. The broken plane is shown in the dark shaded area and the rock bridge zones are shown in white. The location of the sensor array (Figure 4) is indicated by a white translucent parallelogram.

helicopter lidar scans of the cliff were acquired in October and December 2007, before and after the failure, using a Riegl 2-D laser scan brought together with a Hasselband digital camera, an Inertial Measurement Unit iMAR and a dual frequency GNSS receiver. Helicopter scanning allowed the geometry of the column and the morphology of the failure surface to be determined (Figure 3) with an average point spacing of 0.20 m, minimizing the number of uncovered areas.

[10] The column that crashed down was about 90 m high, 30 m wide, and 2–10 m thick. The shape of the failure surface is complex, with two outgrowths on either side of the main area (Figure 3). The top part of the failure surface approaches a nearly perfect vertical plane for 30 m and is smooth compared to the rest of the scar. The remainder of the failure surface presents an overall positive tilt, except for a large overhanging zone at the bottom of the scar. After the collapse, rock bridge positions were visually localized by abseiling down the scar (see path in Figure 2b). Two zones showed evidence of fresh intact rock rupture: an elongated horizontal area corresponding to a 6-m-thick limestone bed located 30 m below the plateau and an elongated, vertical 15-m-high polyhedron area located 75–90 m below the plateau. The lower part of this rupture zone is overhanging. No friction feature was observed on these parts of the failure surface, indicating that they failed under normal tensile stresses. Other rock bridges could have been missed in the southern outgrowth of the rupture failure surface, which was not visible from the abseiling path.

[11] To monitor precursory patterns of the fall, the Chamousset site was equipped with a temporary seismic array from the 13 July 2007 to the 10 October 2007 and two horizontal cable extensometers from the 1 August 2007 to 27 November 2007. The latter were installed inside the tension crack separating the column from the stable rock mass (Figure 4). At the beginning of the monitoring, the crack opening at the surface was about 1 m. The seismic array consisted of seven short-period (2 Hz) seismometers (one with three components and six vertical components). One vertical seismometer was installed on the column, while the other six were deployed on the plateau with an array aperture of about 40 meters. During the last 2 months of record, short-period seismometers were replaced by 4.5 Hz geophones, but only the one installed on the column (C′1) worked properly. The monitoring system recorded in a continuous mode (1000 Hz of sampling frequency), but it stopped working on 10 November 2007, 14 days before the

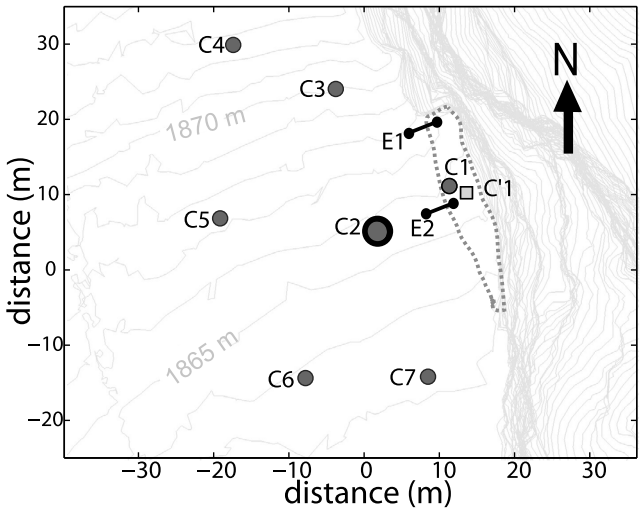

Figure 4. Temporary equipment at Chamousset from July to November 2007. Seven short period seismometers (labeled C1 to C7; dark circles) were deployed from the 13 July 2007 to the 10 October 2007. C2 is a 3-C sensor. One 4.5 Hz geophone (C′1; square) was installed on the column from 01 August 2007 to 26 November 2007. Extensometers E1 and E2 (black segments) were installed from 01 August 2007 to 26 November 2007. Limits of the rock column are shown by the shaded dashed line.

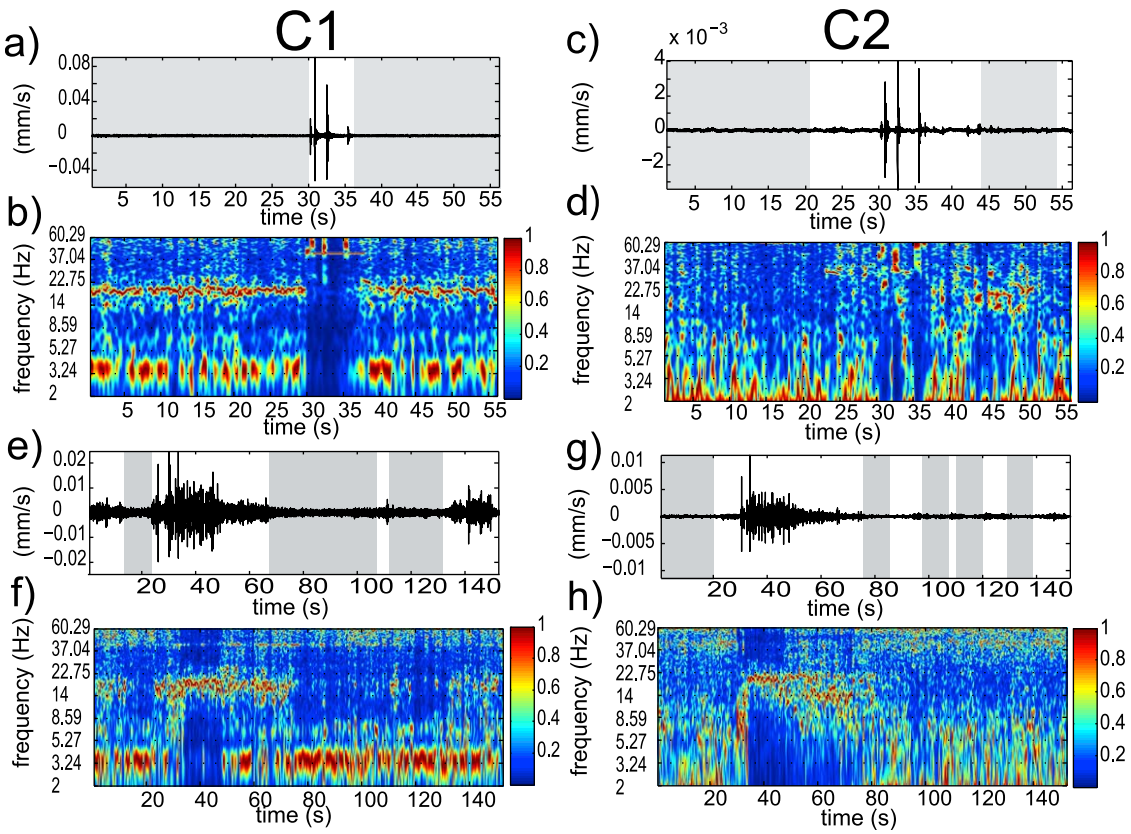

Figure 5. Signals and spectrograms for two types of seismic events. (a) and (b) Impulsive signal recorded on the rock column (vertical seismometer C1) on 25 July 2007 at 03:12:27 and corresponding normalized spectrogram. (c) and (d) The same as Figures 5a and 5b on the rock mass (vertical component of seismometer C2). (e) and (f) Complex signal recorded on the rock column (vertical seismometer C1) on 10 August 2007 at 0202:58 and corresponding spectrogram. (g) and (h) The same as Figures 5e and 5f on the rock mass (vertical component of seismometer C2).

fall, after the solar panels were covered by snow. Owing to maintenance problems at this remote high-elevation site, records were discontinuous with several nonoperating periods. The air temperature and rainfall were recorded by a permanent meteorological station located 3.2 kilometers to the Southwest from the site and 120 m below in altitude.

[12] Geophysical investigation was performed on the plateau after the rock fall. Two 30-m-long seismic profiles were acquired parallel and perpendicular to the cliff in September 2008. A seismic model consisting of a 2 m thick soil layer overlying bedrock was derived from data, with *P* wave and *S* wave velocities of 430 m/s and 180 m/s, respectively, in the soil layer and about 2800 m/s and 960 m/s in the bedrock. These values characterize the material at the scale of the seismic wavelength, in the range of a few tens of meters, considering the rock mass and its discontinuities as an equivalent medium.

3. Data Analysis

[13] During the monitoring period, seismic noise was recorded in a continuous mode, as well as thousands of small seismic events of different types. Figure 5 shows vertical signals and normalized spectrograms recorded simultaneously on the column and on the mass and corresponding to two different types of events. Spectrograms were computed using 1 second windows with 98% of overlap. In the first case (Figures 5a–5d), seismic events are impulsive and much more energetic on the column (Figure 5a) than on the rock mass. The spectrogram on the column (Figure 5b) shows three dominant frequencies at about 3, 7, and 20 Hz in the seismic noise. During the seismic events, the energy shifts to frequencies higher than 40 Hz and the discrete frequency of 40 Hz was continuously excited. On the rock mass, the seismic noise energy is more scattered, but the frequency range exhibits a similar shift to higher frequencies during the seismic events. These impulsive events usually exhibit *P* waves and *S* waves and probably correspond to the local rupture phenomena. In Figure 6 are shown the vertical component on the column and the three components measured on the rock mass. *P* and *S* waves can be easily picked with a time difference of 46 ms. Considering the in situ measured *P* wave and *S* wave velocities leads to a hypocentral distance of about 70 m, which fits with the location of the lower observed fresh rupture surface. Of particular interest is the monofrequency coda at 40 Hz observed in Figure 6a, showing the excitation of the column at that peculiar frequency.

[14] In the second case (Figures 5e–5h), seismic events are less energetic and longer. Motions are still of higher

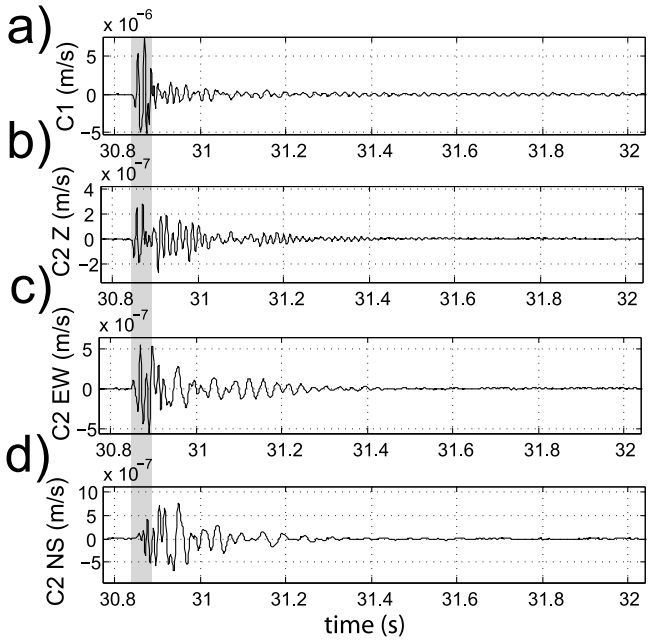

Figure 6. Detail of the transient signal shown in Figure 5 and recorded on (a) the vertical seismometer C1), and on (b) the 3-C seismometer C2 Z, (c) EW and (d) NS on 25 July 2007 at 03:12:27. The shaded window limits indicate the *P* and *S* wave arrivals.

amplitude on the column. On the column (Figure 5f), seismic noise spectra show four dominant frequencies at 3, 7, 20, and 40 Hz, while seismic event spectra exhibit peaks around 20 Hz and at 40 Hz. On the stable rock mass, the noise spectra are again more scattered with, however, the same peaks as on the column. During the main seismic event (Figure 5g), the spectral energy concentrates around 20 Hz before progressively spreading out in the trail of the event. The origin of these seismic event types is still unclear but could correspond to block falls. These observations show that the seismic noise spectra on the column systematically exhibit energy peaks at peculiar frequencies (3, 7, 20, and 40 Hz) which could correspond to some of the column resonance frequencies. These two examples indicate that seismic events of different types were recorded. The events spectra are dominated by higher frequencies with respect to ambient noise spectra, depending on the spectral characteristics of the incoming signal.

[15] This study is focused on the evolution of the column natural frequencies, and the seismic events, which disturb the spectra, were rejected using an antitriggering STA/LTA filter with a threshold ratio of 2 and short and long windows of 0.5 and 20 s, respectively. The time periods fitting this criterion and considered for the spectra computations are shaded in Figure 5.

[16] Spectra were calculated for 5 s time windows and summed over an hour with no smoothing processing for the vertical sensors installed on the column (C1 and C′1; Figure 4). No instrumental correction was applied to the seismograms. Figure 7a shows the evolution of the 1-hour spectra with time, between 24 July and 10 November 2007. Four normalized Fourier spectra curves between 2 Hz and 30 Hz are plotted in the same figure. At the beginning of the monitoring (August 2007), four distinct energy peaks are observed at about 3.6 Hz, 7 Hz, 18 Hz, and around 40 Hz. The peak at 3.6 Hz is by far the most energetic one. Its frequency slightly varies with time between August and the beginning of October and decreases between October and November to reach 2.6 Hz, 15 days before the collapse. In November

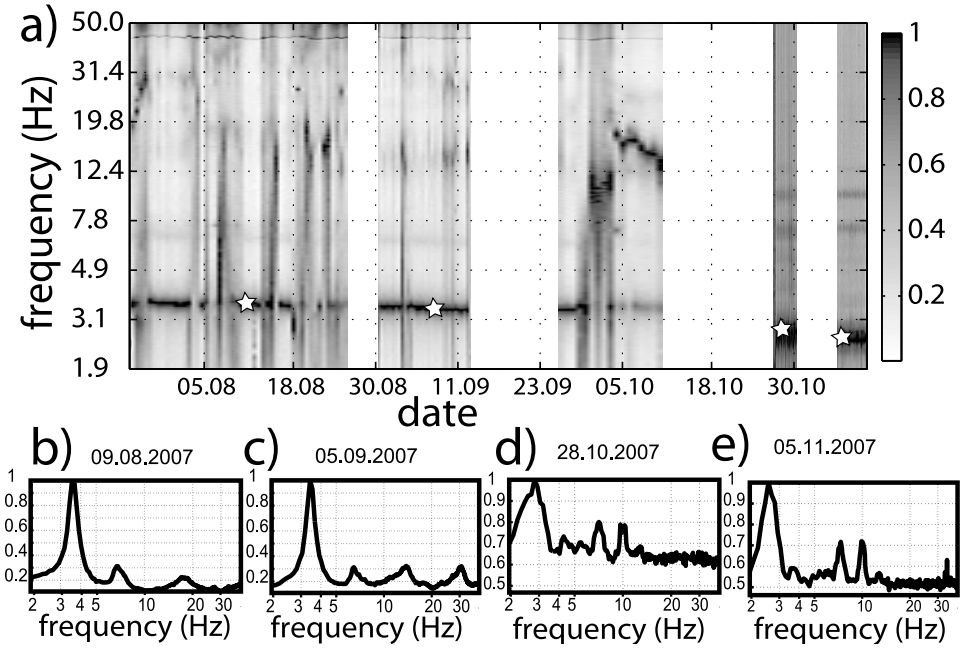

Figure 7. (a) Normalized spectra as a function of time for the vertical seismometer (C1 or C′1) installed on the Chamousset column at the Chamousset site from July to November 2007. Graphs (b), (c), (d) and (e) show the normalized Fourier spectra shapes at the dates indicated with a star in Figure 7a.

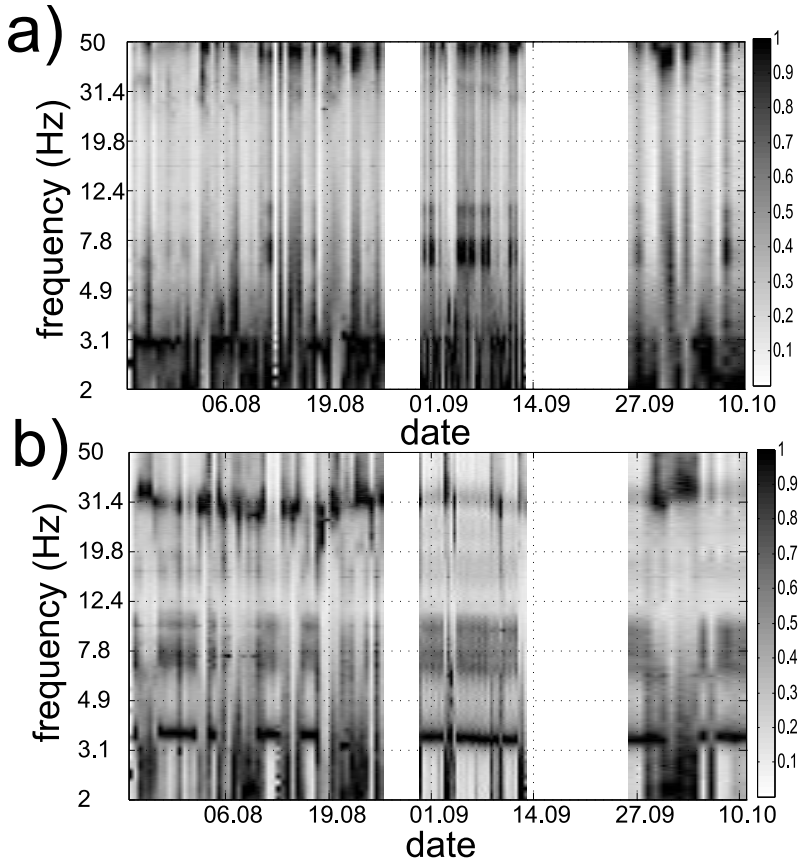

Figure 8. Evolution of the normalized spectra with time for (a) the vertical component of seismometer C2 and (b) the EW horizontal component of seismometer C2.

2007, seismograms were recorded using 4.5 Hz sensors, with a lower sensitivity (32 V/m/s) than the short period one (1920 V/m/s) and a natural frequency above the main peak frequency. Although the corresponding spectra are probably biased, they still show a predominant peak at a low frequency (Figures 7d and 7e) that is consistent with the previous measurements. However, doubt can be raised about this value, and this issue is addressed in the Discussion section.

[17] In Figure 8 are plotted the evolution of the normalized spectra for the vertical and EW components of seismometer C2 installed on the rock mass (Figure 4) between 24 July 2007 and 10 October 2007. Peaks are barely visible on the vertical component of C2 (Figure 8a). Spectra measured on the other vertical sensors deployed on the plateau (not shown) exhibit the same characteristic. On the contrary, the EW component spectra show several peaks between 3 and 40 Hz. Of particular interest is the peak at the lowest frequency (3.6 Hz), which is identical to the one indicated in Figure 7a.

[18] Seismic noise spectra measured on the column show a predominant low frequency which fluctuates with time and seems to decrease before the rock fall. To study these frequency variations in detail, we used the random decrement technique initially proposed by *Cole* [1968] to study the dynamic response of space shuttle wing and later applied in civil engineering by *Asmussen* [1997]. This technique consists of stacking a large number of signal windows starting at zero with a positive slope and deducing the impulse response function of the structure. The principle of the method is to select time windows of a given length inside the noise signal which had been previously filtered around the frequency of interest. Averaging a large number of time windows of the response with the same initial condition contributes to reduce the random part of the response and the noise, allowing the free vibrations to emerge. A minimum of 500 windows is required to ensure the stability of the measurements [*Jeary*, 1997]. In our study, the filtering was designed with a 2–4 Hz frequency band, and one thousand 3 s windows were averaged. In Figure 9, the evolution of the determined resonance frequency is compared to the meteorological data (air temperature, wind speed, and rainfall) and to the extensometer data. On the same figure is also plotted the evolution of the seismic energy measured on the vertical component of sensors C1 and C′1, as well as the cumulated number of seismic events with a STA/LTA higher than 6.

[19] First, the air temperature and resonance frequency curves (Figure 9a) both exhibit a global average decrease over the whole monitoring period, of about 20°C and 1 Hz, respectively. Between 24 July 2007 and 4 September 2007, the two curves correlate very well, with frequency oscillations in phase with weekly temperature variations. Thermomechanical simulations of an increase of temperature on the Chamousset column (not presented here) showed that the related rock dilation results in a closure of the fissure and

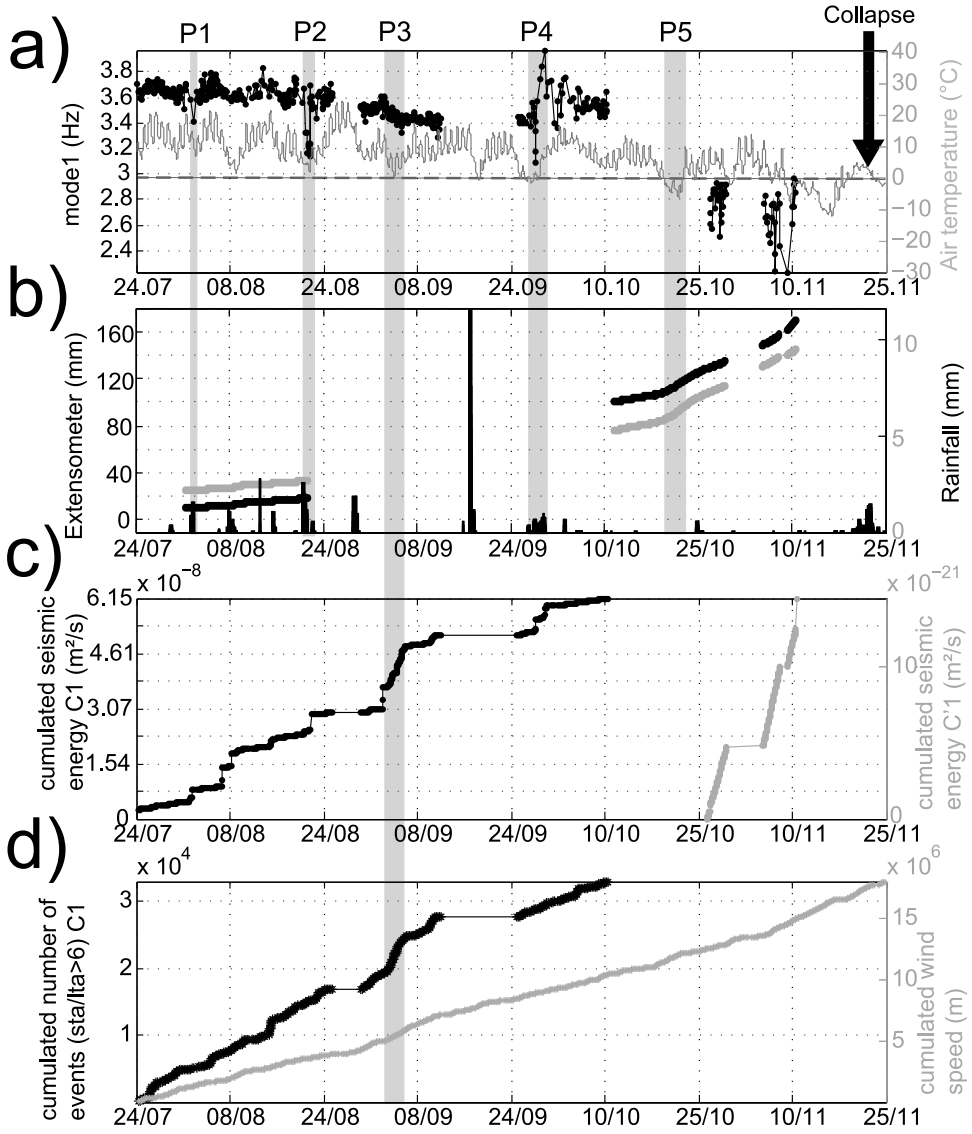

Figure 9. Comparison of seismic data measured for the Chamousset rock column with the meteorological data measured at the "Jardin du Roi" station. (a) Evolution of the lowest resonance frequency (black dot and line) and of the air temperature (shaded line). (b) Evolution of the rear fissure aperture measured by extensometers E1 (black line) and E2 (shaded line) and rainfall data (black bars). (c) Evolution of the seismic energy computed from the vertical signals measured at seismometer C1 (black line) and seismometer C′1 (shaded line) on top of the Chamousset rock column. (d) Evolution of the cumulated number of event with STA/LTA ratios higher than 6 for the seismometer C1 (black line). Evolution of the cumulated wind speed (shaded line).

an increase of the contact surface between the column and the rock mass, explaining the frequency augmentation. From the data, a peak-to-peak variation of 20 °C generated a reversible oscillation of 0.1 Hz in frequency. After 4 September, a peculiar drop in frequency of 0.1 Hz occurred during a period with rising temperature (P3 in Figure 9a), which cannot be explained by meteorological factors (no rainfall and temperature increase period). It coincides with a burst in seismic energy and an increase in the number of seismic events (Figures 9c and 9d), which were interpreted as resulting from the breakage of rock bridges. The wind speed is also slightly higher during that period and probably contributes to excite the column. At the end of September, a dramatic increase of 0.5 Hz in resonance frequency was observed during a rainy period (P4; Figure 9b) and when the temperature fell below zero during a few days (Figure 9a). This effect probably resulted from the development of ice in the fissures, increasing the contact and column stiffness. Finally, the resonance frequency drops of 0.6 Hz between 10 October 2007 and 27 October 2007. This decrease occurred at the same time as a significant temperature drop to −5°C (P5). This freeze-thaw cycle could have contributed to break rock bridges and to lower the resonance frequency. This interpretation is supported by the extensometer data, which both exhibit an increase in displacement rate (Figure 9b) after this temperature drop, from 0.7 mm/day to

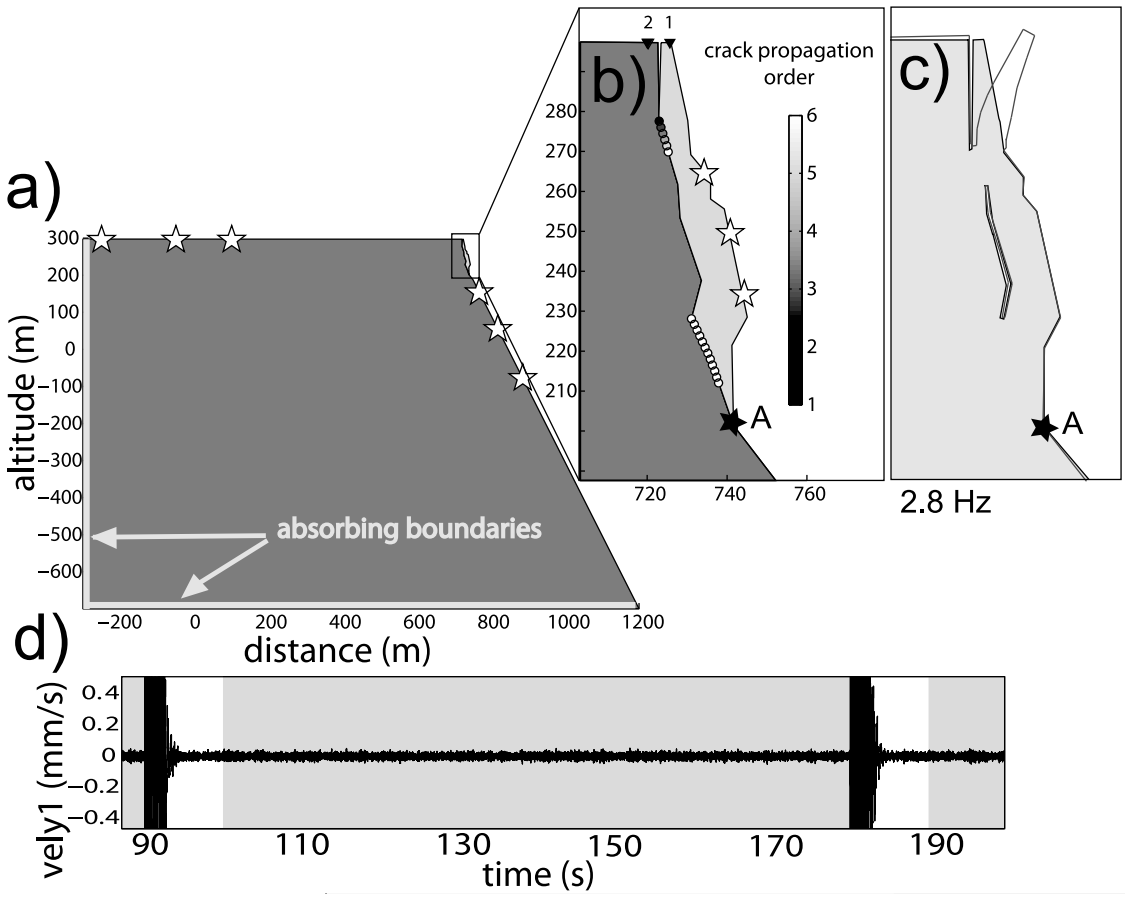

Figure 10. (a) Geometry of the rock mass and of the column, both including a 2 m thick low-velocity layer at the top. White stars stand for seismic noise sources. (b) Cross-section through the Chamousset column with the location of the two sensors (black triangles) and of the two zones of rock bridges along the scar. Filled circles localize ruptures occurring during the simulation. (c) Shape of the column first mode deduced by a 2-D modal analysis using RDM6 software. Rock bridges extension corresponds to the rupture configuration at 230 s during the numerical simulation using the Plast2 software. (d) Vertical velocity signals computed at sensor 1 during two rock bridge cracks. Seismic noise windows used for spectra computations are shaded, while crack-generated signals are indicated by white windows.

more than 3mm/day. Between these two dates, the seismometer characteristics have, however, changed, and this potential influence is addressed in the Discussion section. Several resonance frequency drops (P1, P2, and P4; Figure 9a) coincide with rainfall events (Figure 9b). They could be explained by an increase in weight resulting from water infiltration. However, the cumulated height of water is too small to provoke a significant weight change of the column, except if the rear fissure drains some water from the mass. Moreover, other rainfall events did not appear to cause frequency drops. Another interpretation is that water can decrease the stiffness of the column by lubricating the joints. Finally, the collapse of the column occurred on 24 November 2007, when the temperature became positive after 11 days with negative temperature (Figure 9a).

4. Numerical Modeling of the Chamousset Rock Column

[20] A 3-D modal analysis of the Chamousset rock column was performed using the Finite Element software *Comsol* (http://www.comsol.com). The column geometry was derived from the two lidar data, and clamped boundary conditions were set where fresh rock ruptures were observed (i.e., with a similar rock bridge distribution to the 2-D simulation at 230 s; Figure 10). The 3-D modal analysis showed that the first resonance frequency, around 3 Hz, corresponded to a flexion mode of the 30-m-high upper part of the column, over the horizontal rock bridge zone (Figure 3a). This mode deformation looks like the 2-D mode on Figure 11c. The second and third resonance frequencies (6 Hz and 11 Hz) found by this 3-D analysis correspond to a torsion mode around the rock column vertical axis and a flexion mode along the rear fracture azimuth, respectively. These results confirm that the resonance frequency recorded on site (ranging from 3.6 Hz to 2.6 Hz) corresponds to the first flexion mode of the rock column in a direction perpendicular to the rear fracture. Moreover, measurements of extensometers E1 and E2 (Figure 9) showed that the opening rate evolution was similar along the rear fracture, highlighting the 2-D deformation of the upper part of column. Finally, the lidar

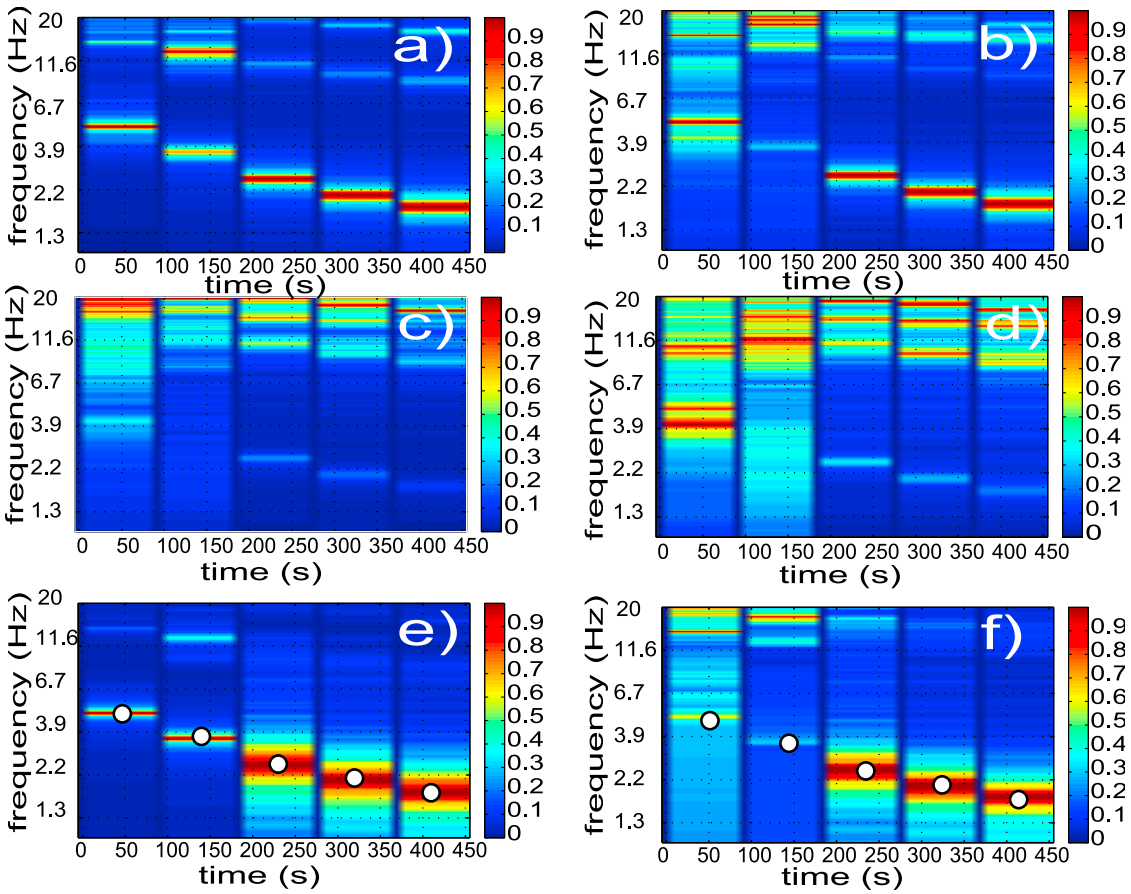

Figure 11. (a) and (b) Normalized spectra computed on the column (seismometer 1) in the horizontal and vertical components, respectively. (c) and (d) Same as Figures 10a and 10b on the rock mass (seismometer 2). (e) and (f) Normalized column-to-mass spectral ratio in the horizontal and vertical directions, respectively. White dots indicate the theoretical frequency for the first resonance mode using the RDM6 software.

DEM shows little lateral variation of the column geometry over the 30 upper meters. The first resonance mode of the column then appears to mainly affect its free upper part, characterized by a 2-D geometry. From these observations and for computation time reasons, we focused our study on the 2-D numerical simulation of the column and on the first mode of resonance, using the hypotheses of planar deformations.

[21] Two-dimensional finite element nonlinear modeling was achieved to mimic the evolution of the first column resonance frequency prior to its collapse. The 2-D elastic column geometry is derived from the lidar data acquired before and after the fall (Figure 3). In the simulation, the 1500-m-wide and 1000-m-high rock mass is limited by absorbing boundaries (Figure 11a).We used the explicit dynamic finite element code Plast2 [*Baillet et al.*, 2005; *Deparis et al.*, 2008b]. The motion equation was both spatially and temporally discretized by using the finite element method and the β_2 explicit time integration scheme [*Carpenter et al.*, 1991], respectively. To ensure stability, the explicit scheme satisfies the Courant-Friedrichs-Levy (CFL) condition ($\Delta t \leq \xi(h/c)_{min}$), where Δt is the time step, h is the element size, c is the wave speed, and ξ is a positive constant ($\xi < 1$, $\xi \approx 0.5$ in most practical purposes). Correct wave propagation was obtained by using 10 finite elements per wavelength [*Mullen and Belytschko*, 1982] with the absorbing boundary conditions proposed by *Stacey* [1988]. Computations were made with 9245 quadrilateral finite elements with a minimum element size h of 0.4 m.

[22] The simulation reproduced the progressive brittle failure of rock bridges along the prone to be broken plane. Rock bridges were set at the two zones along the scar (Figure 11b), where fresh rupture was evidenced during abseiling (Figure 3b). The rest of the interface is subjected to Coulomb friction (μ = 0.7) whenever in contact. Rock bridges are modeled by nodes of the column mesh sticking to the massif surface (Figure 11). During the simulation (Figure 11b), the proportion of rock bridges evolves from 7.3% (i.e., 18 nodes out of 245 along the interface were attached to the mass) to 0%. Rock bridges follow a Mohr-Coulomb criterion ($\tau = C + \sigma_n \tan\varphi$ with $\tan\varphi = 0.7$), and their breakage is managed by decreasing, every 90 s, the cohesion C of the currently most stressed node along the interface until rupture. The contact nonlinearity (column/massif interface) is taken into account by using the Lagrange multiplier method [*Carpenter et al.*, 1991], which enables the evaluation of the normal σ_n and tangential τ contact stresses, as well as the determination of whether the contact

surfaces locally stick, slip, or separate. The contact algorithm uses slave nodes on the column and target surfaces on the massif. An elementary target surface defined by two nodes is broken down into a Ferguson patch with a C^1 continuity across the adjacent boundary [*Faux and Pratt*, 1979]. A model coupling unilateral contact condition, Coulomb friction, and Mohr-Coulomb criterion is used for computing the contact stresses and displacements at each iteration. We set the value of 13 MPa as initial cohesion for the model rock bridges, which was derived from back analysis of rock falls in steep limestone cliffs in the French Alps [*Frayssines and Hantz*, 2009]. After five ruptures at altitudes ranging from 260 m to 280 m, the critical cohesion on the remaining rock bridges exceeded the initial cohesion and led to the column collapse. Values of the Young modulus and Poisson ratio for the bedrock and the upper 2-m-thick weathered layer were derived from the *P* and *S* wave velocities provided by the seismic profiles achieved in September 2008. These moduli and Poisson ratios are representative of the rock mass at the scale of the seismic wavelength (20 m to 40 m) and then take into account the presence of discontinuities in an equivalent medium.

[23] The medium was permanently excited using white noise sources placed at nodes on the surface of the mass and the column (Figures 11a and 11b). At each time step, a random external force is generated at these nodes using the software designed by *Matsumoto and Nishimura* [1998]. Several distributions of the noise sources with different maximum amplitudes were tried: inside the rock mass, along the free surfaces and close to the interface mass column. It turned out that the source location does not influence the results as long as the amplitude and the duration of the excitation are large enough. Synthetic signals were computed at two nodes (Figure 11b) located at the top of the rock mass (sensor 2) and at the column surface (sensor 1). A time lag of 90 s is left between each rupture to select 80-s-long time windows free of rupture effects (Figure 11d). Seismic noise spectra were computed on the 80-s-long time windows between rock bridge ruptures (Figure 10). Those were long enough to adopt the same signal processing as for field seismic data.

[24] The evolution of the normalized spectra with time on the column (sensor 1 in Figure 11b) is shown in Figures 10a and 10b for the horizontal and vertical components, respectively, between 0 and 20 Hz. Spectra simulated on the horizontal component exhibit one predominant energy peak at a low frequency, which consistently decreases with time and the number of broken rock bridges, from 5 Hz to 1.8 Hz. These values encompass the experimental peak frequencies (3.6 to 2.6 Hz), which were interpreted as the lowest resonance frequency of the column. Similar results are obtained along the vertical component (Figure 10b), although with less energy for the two first rock bridge geometries. On the contrary, the energy on the rock mass for both components (Figures 10c and 10d) mainly concentrates at higher frequency (over 10 Hz), although the energy peaks at the column resonance frequency are slightly visible. These peaks result from the transmission of the energy induced by the column vibrations to the rock mass. Vibration amplitudes simulated for further points on the rock mass show that they decrease with distance to the column. This column-to-mass energy transmission was observed at the Chamousset site along the EW component (Figure 8b). Finally, simulated normalized column-to-mass spectral ratios are shown in Figures 10e and 10f in the horizontal and vertical directions. The theoretical frequencies corresponding to the first resonance mode of the column were computed using RDM6 software (http://iut.univ-lemans.fr/ydlogi/rdm_version_6.html) for five rock bridge extensions and are plotted on both graphs. These values perfectly match the predominant peaks derived from the simulated ambient vibrations. Similarly to the spectra results, the ratios along the horizontal component exhibit clearer peaks than along the vertical one, particularly during the first two simulation stages. This results from the greater horizontal displacements generated by the first flexion mode, as illustrated in Figure 11c, and confirms recent observations made by *Burjánek et al.* [2010].

[25] The 2-D dynamic modeling of the Chamousset column, considering the rock bridge location before failure and their progressive breakage, showed that the measured and simulated drops in resonance frequency are in a similar range. The evolution of the resonance frequency with time could then be used as a precursor for monitoring the decoupling of the column from the rock mass before its collapse.

5. Discussion and Conclusions

[26] This paper investigates the variation of the lowest resonance frequency of the Chamousset rock column prior to its collapse, from field measurements and numerical modeling. The comparison of the measured resonance frequency with meteorological data indicates a strong control of the temperature on the frequency values. When the temperature is positive, weekly variations create in-phase reversible resonance frequency oscillations of 0.1 Hz in amplitude, which result from the increase (decrease) of contact stiffness between the column and the rock mass during thermal rock dilation (contraction). The effect of rainfalls is more debatable. A drop of frequency was observed during some of the rainfall events, which could be partly explained by an increase of the column mass owing to an influx of water. No data are, however, available to support this hypothesis. The limestone being highly permeable owing to karstic solution and crack opening, this effect should be very limited in time. Another process could be a decrease of the stiffness due to water lubrication of the joints. The influence of these meteorological factors is reversible and can be combined, leading to opposite or conjugate effects. When the temperature fell below zero after or during a rainy period, the resonance frequency can temporarily increase, as was observed at the end of September 2007. This effect probably results from the formation of ice, which was favored by local continuous water seepage, observed at several sites in the cliff face. In the open rear crack, temperature was close to air temperature and ice could have filled a part of the crack, increasing the contact cohesion between the column and the rock mass. On the other hand, the presence of ice contributes to the irreversible fissure growth, either during the phase change from liquid to solid or during the ice dilation occurring when negative temperatures increase. *Frayssines and Hantz* [2006] demonstrated that freeze-thaw cycles are the main cause of rock falls in such massive limestone cliffs. They observed that

failure often occurred at the end of the freeze-thaw cycle, when the temperature reached positive values and canceled the cohesion effect at the ice-rock interface. This relation was observed before the column collapse at the Chamousset site. One month and a half before the failure, a severe drop in resonance frequency was observed between 10 October 2007 and 27 October 2007. Unfortunately, this drop coincided with a seismometer change and the installation of one 4.5 Hz geophone on the column. Although some doubt can be raised about the spectra quality below the geophone natural frequency, the reliability of the frequency measurements is supported by the following arguments. First, the Fourier spectra (Figures 7d and 7e) exhibit a clear peak with a high energy at a frequency which consistently decreases with time. Second, the temperature significantly fluctuates during that period, with 4 days at −5°C. That major freeze-thaw cycle, which coincides with a significant augmentation in displacement rate, was likely to damage rock bridges and to cause a decrease in resonance frequency, particularly when approaching the failure which occurred 15 days after the last measurement. Studying the triggering factors for rock falls in calcareous cliffs in the French Alps, *Frayssines and Hantz* [2006] identified ice jacking as the main physical process leading to failure. Finally, numerical simulations performed with the 2-D geometry of the Chamousset column and the estimated rock bridge area consistently retrieved the measured resonance frequency range (3.6 to 2.6 Hz). The irreversible resonance frequency decrease observed in November 2007 seems, then, to be consistent both with the meteorological data and the evolution of the column which decouples from the rock mass.

[27] A drop in frequency, which was not linked to temperature variation or rainfall, occurred around 4 September. It coincided with a burst in seismic energy and in wind speed, as well as with the number of seismic events. Strong winds contribute to increase the measured seismic energy but also dynamically excite the column. The concomitant increase of the number of rupture seismic events supports the hypothesis that the frequency drop results from rock bridge breakage, probably partially induced by the wind. An alternative to contact stiffness variation for explaining frequency drops is the decrease of the shear and Young moduli resulting from progressive damage in the rock column itself. Although this effect cannot be ruled out, the consistency between the measured and simulated frequency values, the field observation of one major rear tension crack, and the records of rupture seismic events exhibiting *P* and *S* waves suggest that the reduction of rock bridges is the major factor controlling the observed resonance frequency decrease in this case. Although freeze-thaw cycles have seemed to play a predominant role in the collapse, fissure growth could also have resulted from temperature-independent phenomena such as the wind effect or the tertiary creep [*Kemeny*, 2003].

[28] Both in situ measurements and numerical modeling have shown that the column resonance frequency can be easily derived from ambient vibration study, computing the Fourier spectra of the motion recorded at the column top. The resonance frequencies of the column are, however, enhanced by the computation of the column-to-rock mass spectral ratio, provided that the rock reference station is far enough from the column. Although resonance frequencies were in situ measured with vertical sensors at Chamousset, numerical modeling has indicated that the resonance mode at the lowest frequency (column flexion) is more easily detected on the horizontal component. Moreover, this first resonance frequency, which was measured between 2 and 4 Hz at Chamousset, depends on the column volume and could be lower than 1 Hz for column size of a few tens of thousands m^3. Consequently, the minimum recommended instrumental configuration for such study would be two 3-C low-frequency sensors installed on the column and on the rock mass.

[29] Contrary to other precursors such as surface crack opening, which can manifest only locally, the decrease of resonance frequency with time offers the advantage of being a global parameter characterizing the column mass and its coupling to the stable rock mass. The results of this study suggest that the evolution of lowest natural frequency could be a reliable precursor of rock falls. However, they were obtained for a brittle and strong bedded rock (limestone) with a well-delineated column decoupled from the rock mass. The application of this technique to softer rocks affected by more complex deformation patterns has still to be proved.

[30] **Acknowledgments.** This work was partially funded by the ANR Triggerland, the federative structure VOR (Vulnérabilité des Ouvrages aux Risques) and the Marie Curie Program "Mountain Risks." This work would not have been achieved without the help of many field work participants; we are especially grateful to R. Béthoux and G. Cougoulat, as well as to the rangers of the Vercors Regional Park for drawing our attention to the Chamousset site and for allowing the deployment of a scientific experiment in a protected area. All (or most of) the computations presented in this paper were performed at the "Service Commun de Calcul Intensif de l'Observatoire de Grenoble (SCCI)." The authors are also grateful to the "parc national Sismob (INSU-CNRS)" and the LGIT for the lending of instruments. The authors thank the associate editor as well as Jan Burjánek and two anonymous reviewers for their constructive and helpful comments.

References

Amitrano, D., J. R. Grasso, and G. Senfaute (2005), Seismic precursory patterns before a cliff collapse and critical-point phenomena, *Geophys. Res. Lett.*, *32*, L08314, doi:10.1029/2004GL022270.

Amitrano, D., S. Gaffet, J.-P. Malet, and O. Maquaire (2007), Understanding mudslides through micro-seismic monitoring: The Super-Sauze (South-East French Alps) case study, *Bull. Soc. Géol. France*, *178*(2), 149–157.

Amitrano, D., M. Arattano, M. Chiarle, G. Mortara, C. Occhiena, M. Pirulli, and C. Scavia (2010), Microseismic activity analysis for the study of the rupture mechanisms in unstable rock masses, *Nat. Hazards Earth Syst. Sci.*, *10*, 831–841, doi:10.5194/nhess-10-831-2010.

Asmussen, J. C. (1997), Modal analysis based on the random decrement technique-applications to civil engineering structures, Ph.D. thesis, Aalborg University, Denmark.

Azimi, C., and P. Desvarreux (1996), Quelques aspects de la prévision des mouvements de terrains, *Rev. Franç. Géotech.*, *76*, 63–75.

Baillet, L., V. Linck, S. D'Errico, B. Laulagnet, and Y. Berthier (2005), Finite element simulation of dynamic instabilities in frictional sliding contact, *J. Tribol.*, *127*(3), 652–657.

Burjánek, J., G. Gassner-Stamm, V. Poggi, J. R. Moore, and D. Fäh (2010), Ambient vibration analysis of an unstable mountain slope, *Geophys. J. Int.*, *180*(2), 820–828, doi:10.1111/j.1365-246X.2009.04451.x.

Carpenter, N. J., R. L. Taylor, and M. G. Katona (1991), Lagrange constraints for transient finite element surface contact, *Int. J. Num. Meth. Eng.*, *32*, 130–128.

Clinton, J. F., S. C. Bradford, T. H. Heaton, and J. Favela (2006), The observed wander of the natural frequencies in a structure, *Bull. Seismol. Soc. Am.*, *96*(1), 237–257, doi:10.1785/0120050052.

Cole, H. A. (1968), On-the-line Analysis of Random Vibrations, Structural Dynamics and Materials Conference, AIAA Paper No. 68-288, Palm Springs, Calif., USA.

Crosta, G., and F. Agliardi (2003), Failure forecast for large rock slides by surface displacement measurements, *Can. Geotech. J.*, *40*, 176–191, doi:10.1139/t02-085.

Deparis, J., B. Fricout, D. Jongmans, T. Villemin, L. Effendiantz, and A. Mathy (2008a), Combined use of geophysical methods and remote techniques for characterizing the fracture network of a potential unstable cliff site (Vercors massif, France), *J. Geophys. Eng.*, *5*, 147–157, doi:10.1088/1742-2132/5/2/002.

Deparis, J., D. Jongmans, F. Cotton, L. Baillet, F. Thouvenot, and D. Hantz (2008b), Analysis of rock-fall and rock-fall avalanche seismograms in the French Alps, *Bull. Seismol. Soc. Am.*, *98*(4), 1781–1796, doi:10.1785/0120070082.

Faux, I. D., and M. J. Pratt (1979), Computational geometry for design and manufacture, in *Mathematics and Application*, Elli Horwood Publishers, Chichester, U. K.

Frayssines, M., and D. Hantz (2006), Failure mechanisms and triggering factors in calcareous cliffs of the Subalpine Ranges (French Alps), *Eng. Geol.*, *86*, 256–270, doi:10.1016/j.enggeo.2006.05.009.

Frayssines, M., and D. Hantz (2009), Modelling and back-analysing failures in steep limestone cliffs, *Int. J. Rock Mech. Mining Sci.*, *46*, 1115–1123.

Fukuzono, T. (1985), A new method for predicting the failure time of a slope, in *Proceedings of the 4th International Conference and Field Workshop on Landslides*, pp. 145–150, Tokyo University Press, Tokyo, Japan.

Gaffet, S., Y. Guglielmi, F. Cappa, C. Pambrun, T. Monfret, and D. Amitrano (2010), Use of the simultaneous seismic, GPS and meteorological monitoring for the characterization of a large unstable mountain slope in the southern French Alps, *Geophys. J. Int.*, *182*, 1395–1410, doi:10.1111/j.1365-246X.2010.04683.x.

Gidon, M. (1977), *Carte géologique simplifiée des Alpes occidentales, du Léman à Digne, au 1/250.000°*, Didier-Richard, Bur. de Rech. Geol. et Min., Grenoble, France.

Got, J.-L., P. Mourot, and J. Grangeon (2010), Pre-failure behaviour of an unstable limestone cliff from displacement and seismic data, *Nat. Hazards Earth Syst. Sci.*, *10*, 819–829, doi:10.5194/nhess-10-819-2010.

Hoek, E., and J. W. Bray (1981), *Rock Slope Engineering*, rev. 3rd ed., The Institution of Mining and Metallurgy, pp. 341–351, London, U. K.

Jaboyedoff, M., F. Baillifard, F. Philippossian, and J.-D. Rouiller (2004), Assessing the fracture occurrence using the "weighted fracturing density": a step towards estimating rock instability hazard, *Nat. Hazards Earth Syst. Sci. 4*, 83–93, doi:10.5194/nhess-4-83-2004.

Jeannin, M., S. Garambois, C. Grégoire, and D. Jongmans (2006), Multiconfiguration GPR measurements for geometrical fracture characterization in limestone cliffs (Alps), *Geophysics*, *71*(3), B85–B92, doi:10.1190/1.2194526.

Jeary, A. P. (1997), Damping in structures, *J. Wind Eng. Indus. Aerodyn.*, *72*, 345–355, doi:10.1016/S0167-6105(97)00263-8.

Kemeny, J. (2003), The time-dependent reduction of sliding cohesion due to rock bridges along discontinuities: A fracture mechanics approach, *Rock Mech. Rock Eng.*, *36*(1), 27–38.

Kilburn, C. R. J., and N. D. Petley (2003), Forecasting giant, catastrophic slope collapse: Lessons from Vajont, northern Italy, *Geomorphology*, *54*, 21–32.

Lato, M., J. Hutchinson, M. Diederichs, D. Ball, and R. Harrap (2009), Engineering monitoring of rockfall hazards along transportation corridors: Using mobile terrestrial LiDAR, *Nat. Hazards Earth Syst. Sci.*, *9*, 935–946, doi:10.5194/nhess-9-935-2009.

Matsumoto, M., and T. Nishimura (1998), Mersenne twister: A 623-dimensionally equidistributed uniform pseudorandom number generator, *ACM Trans. Modeling Comput. Simul.*, *8*(1), 3–30, doi:10.1145/272991.272995.

Mertl, S., and E. Brückl (2007), Observation of fracture processes in creeping rock masses by seismic monitoring, in *Proceedings at 11th Congress of the International Society for Rock Mechanics*, Lisbon, Portugal.

Michel, C., P. Gueguen, and P.-Y. Bard (2008), Dynamic parameters of structures extracted from ambient vibration measurements: An aid for the seismic vulnerability assessment of existing buildings in moderate seismic hazard regions, *Soil Dyn. Earthquake Eng.*, *28*, 593–604, doi:10.1016/j.soildyn.2007.10.002.

Mullen, R., and T. Belytschko (1982), Dispersion analysis of finite element semi discretizations of the two dimensional wave equation. *Int. J. Num. Methods. Eng.*, *18*, 11–29.

Oppikofer, T., M. Jaboyedoff, and H.-R. Keusen (2008), Collapse of the eastern Eiger flank in the Swiss Alps, *Nat. Geosci.*, *1*, 531–535, doi:10.1038/ngeo258.

Oppikofer, T., M. Jaboyedoff, L. Blikra, and M. Derron (2009), Characterization and monitoring of the Åknes rockslide using terrestrial laser scanning, *Nat. Hazards Earth Syst. Sci.*, *9*, 1003–1019, doi:10.5194/nhess-9-1003-2009.

Petley, D. N. (2004), The evolution of slope failures: Mechanisms of rupture propagation, *Nat. Hazards Earth Syst. Sci.*, *4*, 147–152, doi:10.5194/nhess-4-147-2004.

Roch, K. H., W. Chwatal, and E. Bräuckl (2006), Potential of monitoring rock fall hazards by GPR: Considering as example of the results of Salzburg, *Landslide*, *3*, 87–94, doi:10.1007/s10346-005-0026-8.

Rosser, N., M. Lim, D. Petley, S. Dunning, and R. Allison (2007), Patterns of precursory rockfall prior to slope failure, *J. Geophys. Res.*, *112*, F04014, doi:10.1029/2006JF000642.

Saito, M., and H. Uezawa (1961), Failure of soil due to creep, in *Fifth International Conference of Soil Mechanics and Foundation Engineering*, pp. 315– 318, Montréal, QC, Canada.

Senfaute, G., A. Duperret, and J. A. Lawrence (2009), Micro-seismic precursory cracks prior to rock-fall on coastal chalk cliffs: a case study at Mesnil-Val, Normandie, NW France, *Nat. Hazards Earth Syst. Sci.*, *9*(5), 1625–1641, doi:10.5194/nhess-9-1625-2009.

Sornette, D., A. Helmstetter, J. V. Andersen, S. Gluzman, J.-R. Grasso, and V. Pisarenko (2004), Towards landslide predictions: Two case studies, *Physica A*, *338*(3–4), 605–632, doi:10.1016/j.physa.2004.02.065.

Spillmann, T., H. R. Maurer, B. Heincke, H. Willenberg, and A. G. Green (2007), Microseismic monitoring of an unstable rock mass, *J. Geophys. Res.*, *112*, B07301, doi:10.1029/2006JB004723.

Stacey, R. (1988), Improved transparent boundary formulations for the elastic-wave equation, *Bull. Seismol. Soc. Am.*, *78*, 2089–2097.

Sturzenegger, M., and D. Stead (2009), Quantifying discontinuity orientation and persistence on high mountain rock slopes and large landslides using terrestrial remote sensing techniques, *Nat. Hazards Earth Syst. Sci.*, *9*, 267–287, doi:10.5194/nhess-9-267-2009.

Voight, B. (1989), A relation to describe rate-dependent material failure, *Science*, *243*, 200–203.

Voight, B., and B. A. Kennedy (1979), Slope failure of 1967–1969, Chuquicamata Mine Chile, in *Rock slides & avalanches*, edited by B. Voight, pp. 595–632, Developments in Geotechnical Engineering, 14b, Elsevier, Amsterdam.

Walter, M., and M. Joswig (2008), Seismic monitoring of fracture processes generated by a creeping landslide in the Vorarlberg Alps, *First Break*, *26*(6), 131–135.

Walter, M., and M. Joswig (2009), Seismic characterization of slope dynamics caused by softrock-landslides: The Super-Sauze case study, in *Proceedings of the International Conference on Landslide Processes: From geomorphologic mapping to dynamic modelling*, edited by J.-P. Malet et al., pp. 215–220, CERG Editions, Strasbourg, France.

Wu, L., S. Liu, Y. Wu, and C. Wang (2006), Precursors for rock fracturing and failure Part I: IRR image abnormalities, *Int. J. Rock Mech. Mining Sci.*, *43*, 473–482, doi:10.1016/j.ijrmms.2005.09.002.

Zvelebil, J., and M. Moser (2001), Monitoring based time-prediction of rock falls: Three case-histories, *Physics and Chemistry of the Earth, Part B: Hydrology, Oceans and Atmosphere*, *26*(2), 159–167, doi:10.1016/S1464-1909(00)00234-3.

L. Baillet, D. Hantz, D. Jongmans, and C. Lévy, Laboratoire de Géophysique Interne et Tectonophysique, CNRS, Grenoble University, France. (laurent.baillet@ujf-grenoble.fr)

P. Mourot, Myotis Society, 20, Rue du Tour de l'Eau, Parc Chephren, F-38400 Saint Martin d'Hères, France.